Search for resonances in light-by-light scattering using the forward proton detectors at the LHC-ATLAS

G. Tateno, on behalf of the ATLAS Collaboration
ICEPP, The University of Tokyo - Tokyo, Japan

Summary. — A search for light-by-light scattering mediated by an axion-like particle at the LHC is presented, using the central ATLAS detector to detect pairs of outgoing photons and the ATLAS Forward Proton spectrometer to detect scattered intact protons which produce the photons. Proton–proton collision data recorded in 2017 at a centre-of-mass energy of $\sqrt{s} = 13$ TeV were analysed, corresponding to an integrated luminosity of 14.6 fb^{-1}. A total of 441 candidate events were selected. A search was made for a narrow resonance in the diphoton mass distribution, corresponding to an axion-like particle (ALP) with mass in the range 150–1600 GeV. No excess is observed above a smooth background. Upper limits on the production cross section of a narrow resonance are set as a function of the mass, and are interpreted as upper limits on the ALP production coupling constant.

ATL-PHYS-PROC-2023-051
12 September 2023

1. – Introduction

Some extensions to the Standard Model (SM) predict the possibility of axion-like heavy particles in that they couple to two photons. Such axion-like particles (ALPs) may be produced in two-photon collisions and subsequently decay into two photons [1, 2, 3]; the ALP production process can therefore be identified as a resonant peak at the ALP mass value in the process $\gamma\gamma \to \gamma\gamma$, also known as light-by-light ($\gamma\gamma$) scattering.

At the LHC, substantial fluxes of quasi-real photons can be generated by radiation from colliding high-energy protons or ions, and pairs of such photons can interact. In processes of this kind, each incoming charged particle continues to travel close to its original direction. The process $\gamma\gamma \to \gamma\gamma$ can also occur through an intermediate fermion or W boson box diagram. It has been measured at the LHC in nucleus–nucleus collisions using lead-ion beams (Pb–Pb collisions) [4, 5, 6, 7], where the $\gamma\gamma \to \gamma\gamma$ cross section is enhanced because of the high nuclear charge. These analyses also searched for an ALP mediated by $\gamma\gamma$ scattering with a mass m_X up to 100 GeV. At higher diphoton masses, the effective $\gamma\gamma$ luminosity in pp collisions surpasses that of Pb–Pb collisions [8], although the scattering cross section is lower than at lower masses.

A pair of outgoing real photons, which is the signature for ALP production, can be detected in the central detector surrounding the interaction point, while suitable

apparatus located in each of the forward directions may be used to detect the outgoing scattered protons (referred to as proton tagging) in pp collisions [2]. The production of lepton pairs by photon–photon interactions, $pp \to p(\gamma\gamma \to \ell^+\ell^-)p^{(*)}$, has been measured by ATLAS and CMS using forward-proton detectors [9, 10].

This analysis presents a search for ALPs produced in light-by-light scattering in proton–proton (pp) collisions using the ATLAS detector. The target mass range is 150–1600 GeV. Three possibilities for the reaction are considered: the exclusive process $\gamma\gamma \to \gamma\gamma$ measured as $pp \to pp\gamma\gamma$, and single- and double-dissociative processes (SD, DD) in which one or both protons (p^*) dissociate while radiating a virtual photon, as depicted in fig. 1. While the undissociated proton may be tagged, the dissociated proton is in practice not measurable.

An exclusive signal search has been performed by the CMS–TOTEM collaborations in 9.4 fb^{-1} of pp collisions at $\sqrt{s} = 13$ TeV, making use of double proton tagging in a diphoton mass range of approximately 900–1800 GeV [11]. A previous inclusive diphoton resonance search with ATLAS targeted the mass range 160–1160 GeV using a higher integrated luminosity, 139 fb^{-1} [12]. The ATLAS search presented here uses 14.6 fb^{-1} of 13 TeV pp collision data and requires at least one tagged proton, giving a more specific measurement of the exclusive and SD processes, covering a mass range 150–1600 GeV, and with higher experimental acceptance than in the pure double-tagging case. More details about this analysis can be found in refs. [13, 14].

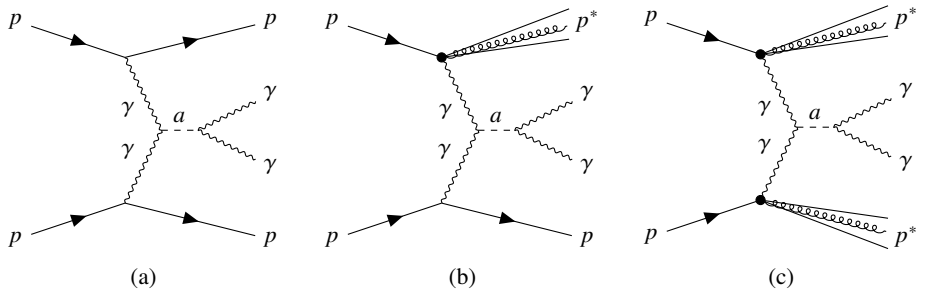

Fig. 1. – Feynman diagrams for (a) exclusive, (b) single-dissociative, and (c) double-dissociative light-by-light scattering with outgoing photon pairs mediated by an ALP denoted by a [13].

2. – Event samples and selection

The ATLAS detector [15] at the LHC is a multipurpose particle detector with forward/backward-symmetric cylindrical geometry and near 4π coverage in solid angle.(1) It consists of an inner tracking detector surrounded by a thin superconducting solenoid providing a 2 T axial magnetic field, electromagnetic (EM) and hadron calorimeters, and

(1) ATLAS uses a right-handed coordinate system with its origin at the nominal interaction point (IP) in the centre of the detector and the z-axis along the beam pipe. The x-axis points from the IP to the centre of the LHC ring, and the y-axis points upwards. Cylindrical coordinates (r, ϕ) are used in the transverse plane, ϕ being the azimuthal angle around the z-axis. The pseudorapidity is defined in terms of the polar angle θ as $\eta = -\ln\tan(\theta/2)$. Angular distance is measured in units of $\Delta R \equiv \sqrt{(\Delta\eta)^2 + (\Delta\phi)^2}$.

a muon spectrometer.

Forward scattered protons are detected in the ATLAS Forward Proton (AFP) spectrometer system [16, 17]. These detectors are positioned near the outgoing proton beam and can be moved in the x-direction close to the beam as required. The AFP spectrometer consists of four tracking units located at $z = \pm 205$ m and ± 217 m. They are denoted as NEAR and FAR stations, respectively, with the $+z$ ($-z$) direction denoted as the A(C)-side. Each station houses a silicon tracker comprising four planes of silicon pixel sensors.

A two-level trigger system is used to select events. The first-level trigger is implemented in hardware and makes use of a subset of the detector information to accept events at a rate below 100 kHz. It is followed by a software-based trigger that reduces the average accepted event rate to 1 kHz. No trigger with an AFP signal was used because each AFP station reconstructs proton tracks with a probability of around 70% per bunch crossing, while new triggers may be added in a future analysis using time-of-flight detectors housed in the AFP FAR stations to reduce the background events.

The dataset was collected in 2017 using pp collisions at a centre-of-mass energy $\sqrt{s} = 13$ TeV. The integrated luminosity was 14.6 fb^{-1}, corresponding to the time the AFP system was in operation together with the central detector and after data-quality requirements. The data were recorded using a diphoton trigger that required two clusters of EM calorimeter cells with transverse energies $E_{\mathrm{T}} = E \sin\theta$ above 35 GeV and 25 GeV, respectively [18, 19], after which standard data-quality requirements were applied [20]. For the forward-proton measurement, it was required that every AFP station had at least three operational silicon planes, with correct operation of the AFP data acquisition system [21].

Simulated signal events were produced using the SUPERCHIC 4.02 Monte Carlo (MC) generator [22, 23, 24] for the exclusive signals and SUPERCHIC 4.14 [3] for the SD and DD signals. ALP masses in the range $m_X = 150$–1600 GeV were considered, and for each m_X value a sample was generated with the ALP-to-diphoton coupling constant set to([2]) $f^{-1} = 0.05$ TeV^{-1}, where the natural width of the ALP is $\Gamma = m_X^3/4\pi f^2$. Generator-level selections were applied, requiring photons to have transverse momentum $p_{\mathrm{T}} > 20$ GeV and $|\eta| < 2.4$; the diphoton rapidity is required to be $|y_{\gamma\gamma}| < 2.4$. The acceptance A_0 for signal events to pass these fiducial region requirements is in the range 60%–75%, depending on m_X. Typically, the SD production cross section is approximately three times the exclusive cross section. To model the central-detector response, the signal samples were processed with a fast simulation [25, 26]. The response of the AFP spectrometer in the MC samples was modelled by a simulation in which Gaussian smearing, based on the AFP spatial resolution, is applied to the generated proton position in each AFP station. The track is then reconstructed according to the simulated positions and subsequently used in the proton reconstruction. The reconstruction of scattered protons in the data combines information from the AFP tracker and knowledge of the LHC magnet lattice [9, 27], which is used to calculate the proton transport from the IP.

Photon candidates were reconstructed from topological clusters [28] of energy deposits in the ATLAS EM calorimeter and were calibrated as described in ref. [29]. To improve the object quality, photon candidates were required to fulfil identification criteria and isolation requirement [30, 29]. The event selection required at least two photon candidates

([2]) f^{-1} is taken from ref. [2], and the input coupling constant parameter of SUPERCHIC is $g_a = 4f^{-1}$ [23, 3].

with $p_{\mathrm{T}} > 40$ GeV and $|\eta| < 2.37$, matched to the online photon objects that triggered the event, excluding the barrel-to-endcap transition regions of the calorimeter, $1.37 < |\eta| < 1.52$. The azimuthal misalignment between the pair of photons was required to be small, as determined by an acoplanarity $A_{\phi}^{\gamma\gamma} = 1 - |\Delta\phi_{\gamma\gamma}|/\pi < 0.01$.

Protons transported to the AFP by the beamline magnets leave hits in its silicon trackers, which are processed by per-plane clustering and per-station track-finding algorithms [31]. Tracks are reconstructed from clusters found in at least two planes in each station. From the track spatial coordinates, the proton energy and momentum at the IP are inferred, using the known beam optics. The result of the reconstruction is the fractional energy loss of the scattered proton, defined as $\xi = 1 - E_{\mathrm{scattered}}/E_{\mathrm{beam}}$, where $E_{\mathrm{scattered}}$ (E_{beam}) is the scattered (beam) proton energy. The determination of ξ from the AFP stations (ξ_{AFP}) requires tracks in both the NEAR and FAR stations. Events with at least one A-side or C-side tagged proton were accepted, for which the ξ_{AFP} value was required to be within the range $[0.035, 0.08]$. A combination of such single proton tagging and double tagging may be considered in the future.

The ξ value of the forward scattered proton can also be calculated independently of the forward protons, using the kinematics of the central photon pair, and is denoted by $\xi_{\gamma\gamma}$. It is determined from the diphoton mass $m_{\gamma\gamma}$ and rapidity $y_{\gamma\gamma}$ by momentum conservation as $\xi_{\gamma\gamma}^{\pm} = (m_{\gamma\gamma}/\sqrt{s})\, \mathrm{e}^{\pm y_{\gamma\gamma}}$, where $+$ ($-$) corresponds to the proton on the A(C)-side and negligible transverse momentum transfer to the protons is assumed. Proton-tagged diphoton candidates were then selected by requiring kinematic matching on at least one AFP side: $|\Delta\xi| = |\xi_{\mathrm{AFP}} - \xi_{\gamma\gamma}| < \xi_{\mathrm{th}}$, where $\xi_{\mathrm{th}} = 0.004 + 0.1\xi_{\gamma\gamma}$. The second term in ξ_{th} takes account of the uncertainty in the proton propagation through the beam optics between the central detector and the AFP spectrometer, which is proportional to $\xi_{\gamma\gamma}$.

3. – Statistical modelling and procedure

For signal events, the diphoton invariant-mass distribution is expected to peak close to the mass of the ALP, with a spread given by the experimental resolution. For the ALP parameters of interest in this analysis, the ALP intrinsic decay width is narrow enough to be ignored. The experimental resolution of the invariant mass is modelled with a double-sided Crystal Ball (DSCB) function [32, 33]. The six parameters of the DSCB function are determined using the simulated signal MC samples. Each parameter is expressed as a linear function of m_X. The signal fiducial cross section, σ_{fid}, and the signal selection efficiency are also modelled as functions of m_X to derive exclusion upper limits for the cross section. The model for the exclusive signal is illustrated in fig. 2(a). The combination of the AFP geometrical acceptance and the $y_{\gamma\gamma}$ distribution of the expected signal gives rise to a double-peaked mass structure in the signal efficiency, which follows from the acceptance values integrated over the mass contours overlapping with the yellow region in fig. 3.

The dominant source of background after the full event selection arises when a pair of photons (or hadronic jets misidentified as photons) is produced in a *pp* interaction other than that giving the detected forward proton but within the same bunch crossing. The protons originate from soft-scale events, in most cases single-diffractive processes. These recorded events are collectively referred to as combinatorial backgrounds and are modelled using a fully data-driven method. An event sample, referred to as a "mixed-data" sample, was constructed by replacing the AFP data from a given event by that from one or more other data events, before the event selection. To maximise the statistical precision, this reassignment was performed using the method described in ref. [9]. All

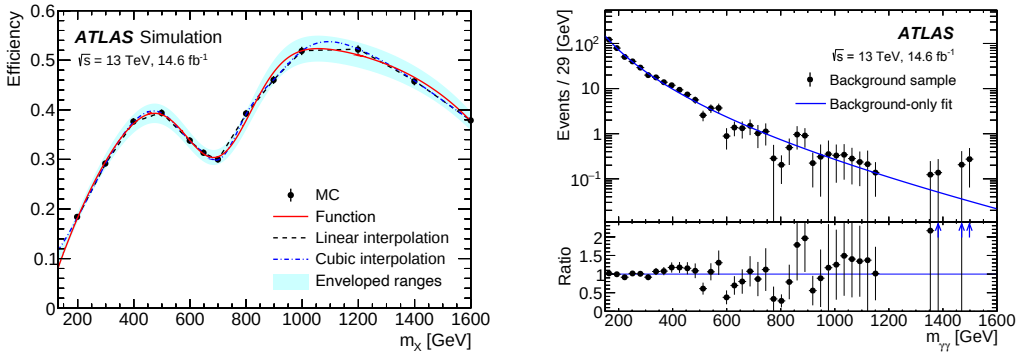

(a) (b)

Fig. 2. – (a) Signal selection efficiency as a function of ALP mass m_X for the exclusive process [13]. The ratio of the number of selected events to the number of generated MC events is given (black points) and is parameterised by an analytic function (red solid line). The linear (black dashed line) and cubic (blue chain line) interpolations of the black points are used to derive the envelopes (cyan filled region) which are regarded as systematic uncertainties. (b) Comparison of the $m_{\gamma\gamma}$ distributions after the full nominal event selection, showing the mixed-data sample (black points) and the background function fitted to it (blue line) in the diphoton mass range $[150, 1600]$ GeV [13]. The ratio of the mixed-data to the fitted function is shown in the lower panel.

possible combinations of diphoton and AFP data from different events within intervals of measured instantaneous luminosity are used, and any contribution from signal events and from background events with a single vertex is suppressed. The normal event selection was then applied to the mixed-data sample, and the events were subsequently inversely weighted by the number of reassignments that were taken for a given diphoton event. This maximal use of proton reassignment gives a mixed-data sample after the kinematic matching that has a distribution in $m_{\gamma\gamma}$ that is as statistically precise as before the matching. A fit was performed to the mixed-data sample using the background distribution function

$$f\left(x; b, a_0\right) = N\left(1 - x^{1/3}\right)^b x^{a_0}, \tag{1}$$

where N, b and a_0 are free parameters to be fitted, and $x = m_{\gamma\gamma}/\sqrt{s}$. This function is a member of a family of functions used in previous diphoton resonance searches [34, 12]. Fig. 2(b) shows the diphoton mass distribution of the mixed-data sample and the fitted result of the background function being used as the initial values of the background function parameters. To evaluate the background-modelling uncertainty, the procedure in ref. [35] was followed. Contributions from backgrounds other than the combinatorial background, collectively referred to as single-vertex backgrounds, were investigated using dedicated MC samples and found to have small effects on the analysis result.

The statistical analysis uses unbinned maximum-likelihood fits made to the $m_{\gamma\gamma}$ distribution using the DSCB signal function and the background function defined in eq. (1). All the parameters of the background function are free parameters. In these fits, the statistical uncertainty dominates over the systematic uncertainty. The systematic uncertainties on the signal function parameters are accounted for in the fits by using nuisance

parameters constrained by Gaussian penalty terms in the likelihood function. The uncertainty of AFP global alignment, the distance between the AFP edge and the beamline, is the largest component of the signal yield systematic uncertainty. Some explanation about the AFP alignment can be found in refs. [9, 13, 14].

Statistical tests were performed in the search range $m_X = 150$–1600 GeV, using the conventional test statistics q_0 for significance and $\tilde{q}_\mu$ for exclusion upper limits [36]. The tests were performed in steps of 4 GeV in m_X. Local p-values and their significance for the background-only hypothesis were calculated using pseudo-experiments for the q_0 distribution. Global significance values were computed using the same pseudo-experiment samples to account for the look-elsewhere effect [37, 38]. The maximum q_0 with respect to m_X, denoted $q_0^{\max}$, was calculated for each pseudo-experiment, and the $q_0^{\max}$ distribution was used to obtain the global p-value.

Pseudo-experiments were used to derive the expected and observed 95% confidence level (CL) exclusion upper limits on the fiducial cross section times branching ratio into two photons, computed using a modified frequentist approach, $\mathrm{CL_s}$ [39, 40].

4. – Results

A total of 441 events are observed in the range $m_{\gamma\gamma} \in [150, 1600]$ GeV. Fig. 3 shows $\xi^+_{\gamma\gamma}$ vs $\xi^-_{\gamma\gamma}$ for these events with $m_{\gamma\gamma}$ and $y_{\gamma\gamma}$ contours. In this sample, 219 (222) events passed the matching selection for the A(C)-side; no event passed the matching for both the A-side and C-side, in accordance with expectations. The highest-mass diphoton candidate observed in the data has a mass of 1.16 TeV. The probability of compatibility with the background-only hypothesis, quantified as the local p-value, is calculated as a function of the hypothesised ALP resonance mass. The most significant excess, observed at $m_X = 454$ GeV, has a local significance of 2.51σ. The global p-value for the null hypothesis is larger than 0.5, from which it is concluded that no significant excess over the background-only hypothesis is observed.

The observed and expected upper limits on the fiducial cross section and coupling constant for ALP production at 95% confidence level, assuming a 100% decay branching ratio into two photons, are shown in fig. 4 and are in good agreement, consistent with the absence of a signal. The upper limits on the coupling constant are derived using the relationship between the expected fiducial cross section and coupling constant in ref. [2]. The observed limit on the coupling constant is in the range 0.04–0.09 TeV^{-1}. A comparison of the result with a previous inclusive diphoton resonance search [12] is described in ref. [13]. The ALP natural width is $\Gamma \approx 1$ GeV for $m_X = 1400$ GeV and $\Gamma \approx 3$ GeV for $m_X = 1600$ GeV at the observed limit. Such widths are sufficiently small to be ignored, relative to the detector resolution. The exclusion of a coupling constant f^{-1} much larger than illustrated by the Γ contours is not justified in this analysis because it violates the narrow-width approximation used in the signal modelling.

5. – Conclusion

A search for an axion-like particle (ALP) has been carried out with the ATLAS experiment using 14.6 fb^{-1} of $\sqrt{s} = 13$ TeV pp collisions at the LHC. Events with centrally produced photon pairs tagged by forward scattered protons have been studied in a search for light-by-light scattering, $pp \to p(\gamma\gamma \to \gamma\gamma)p^{(*)}$, mediated by an ALP resonance. The search was performed in the diphoton mass range $m_{\gamma\gamma} = [150, 1600]$ GeV. No signal is observed, and the data are consistent with a smooth combinatorial background that

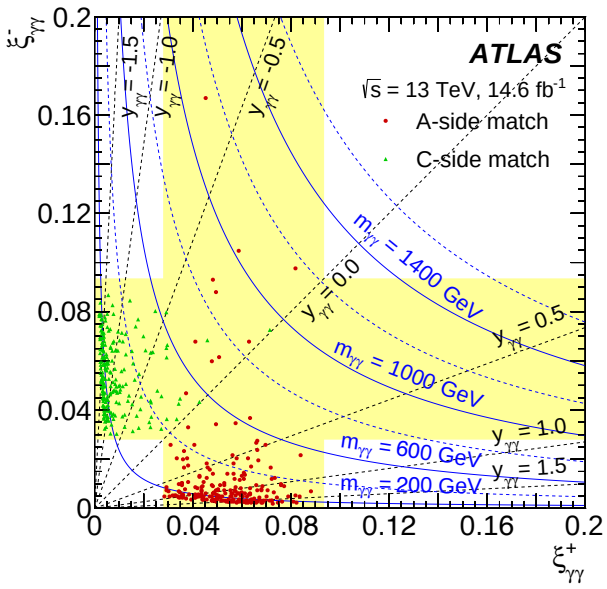

Fig. 3. – $(\xi^+_{\gamma\gamma}, \xi^-_{\gamma\gamma})$ distribution of the selected data candidates after the full event selection in $m_{\gamma\gamma} \in [150, 1600]$ GeV with $m_{\gamma\gamma}$ contours (blue) and $y_{\gamma\gamma}$ contours (black) [13]. The range of $\xi_{\gamma\gamma}$ in which forward-proton matching is possible, $[0.035 - \xi_{\rm th}, 0.08 + \xi_{\rm th}]$, is indicated by the yellow rectangle for each side. Events passing the matching requirement on the A(C)-side are represented by the red dots (green triangles). No event passed the matching requirement for both the A-side and C-side.

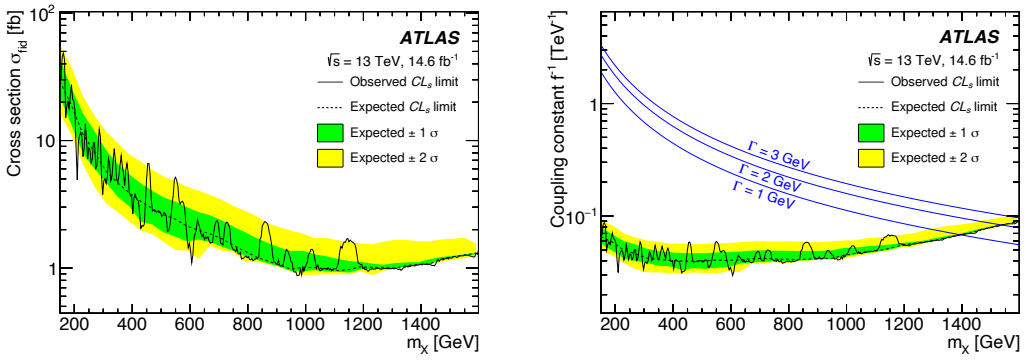

(a) (b)

Fig. 4. – Expected and observed 95% CL upper limits on (a) the signal fiducial cross section $\sigma_{\rm fid}$ and (b) the ALP coupling constant, assuming 100% branching ratio for ALP decay into two photons, as functions of the hypothetical ALP mass m_X [13]. The 1σ and 2σ confidence intervals are shown by the coloured bands. Contours of the ALP natural width Γ are illustrated by the smooth blue solid lines.

can be assumed to come from Standard Model processes. The inferred upper limit on the ALP coupling constant, assuming a 100% decay branching ratio into two photons, is in the range 0.04–0.09 TeV^{-1} at 95% confidence level. These results are comparable to those of the CMS-TOTEM collaboration, obtained using a similar approach, and extend their measured mass range to lower values. More details about the analysis presented here can be found in refs. [13, 14].

REFERENCES

[1] Knapen S., Lin T., Lou H. K. and Melia T., *Phys. Rev. Lett.*, **118** (2017) 171801.
[2] Baldenegro C., Fichet S., von Gersdorff G. and Royon C., *JHEP*, **06** (2018) 131.
[3] Harland-Lang L. A. and Tasevsky M., *Phys. Rev. D*, **107** (2023) 033001.
[4] ATLAS Collaboration, *Nature Phys.*, **13** (2017) 852.
[5] CMS Collaboration, *Phys. Lett. B*, **797** (2019) 134826.
[6] ATLAS Collaboration, *Phys. Rev. Lett.*, **123** (2019) 052001.
[7] ATLAS Collaboration, *JHEP*, **03** (2021) 243.
[8] Bruce R., *et al.*, *J. Phys. G*, **47** (2020) 060501.
[9] ATLAS Collaboration, *Phys. Rev. Lett.*, **125** (2020) 261801.
[10] CMS Collaboration, *JHEP*, **07** (2018) 153.
[11] CMS Collaboration, *Phys. Rev. Lett.*, **129** (2021) 011801.
[12] ATLAS Collaboration, *Phys. Lett. B*, **822** (2021) 136651.
[13] ATLAS Collaboration, *JHEP*, **07** (2023) 234.
[14] Tateno G., CERN-THESIS-2023-006 (2023).
[15] ATLAS Collaboration, *JINST*, **3** (2008) S08003.
[16] ATLAS Collaboration, ATLAS-TDR-024; CERN-LHCC-2015-009 (2015).
[17] ATLAS Collaboration, ATL-PHYS-PUB-2017-012 (2017).
[18] ATLAS Collaboration, ATL-DAQ-PUB-2018-002 (2018).
[19] ATLAS Collaboration, *Eur. Phys. J. C*, **80** (2020) 47.
[20] ATLAS Collaboration, *JINST*, **15** (2020) P04003.
[21] Kocian M., *JINST*, **12** (2017) C01077.
[22] Harland-Lang L. A., Khoze V. A. and Ryskin M. G., *Eur. Phys. J. C*, **76** (2016) 9.
[23] Harland-Lang L. A., Khoze V. A. and Ryskin M. G., *Eur. Phys. J. C*, **79** (2019) 39.
[24] Harland-Lang L. A. *et al.*, *Eur. Phys. J. C*, **80** (2020) 925.
[25] ATLAS Collaboration, *Eur. Phys. J. C*, **70** (2010) 823.
[26] ATLAS Collaboration, ATL-PHYS-PUB-2010-013 (2010).
[27] Staszewski R. and Chwastowski J., *Nucl. Instrum. Meth. A*, **609** (2009) 136.
[28] ATLAS Collaboration, *Eur. Phys. J. C*, **77** (2017) 490.
[29] ATLAS Collaboration, *JINST*, **14** (2019) P12006.
[30] ATLAS Collaboration, *Eur. Phys. J. C*, **79** (2019) 639.
[31] Lange J. *et al.*, *JINST*, **11** (2016) P09005.
[32] ATLAS Collaboration, *Phys. Rev. Lett.*, **113** (2014) 171801.
[33] Oreglia M., SLAC-R-236 (1980).
[34] ATLAS Collaboration, *JHEP*, **09** (2016) 001.
[35] ATLAS Collaboration, *Phys. Rev. D*, **90** (2014) 112015.
[36] Cowan G., Cranmer K., Gross E. and Vitells O., *Eur. Phys. J. C*, **71** (2011) 1554.
[37] Gross E. and Vitells O., *Eur. Phys. J. C*, **70** (2010) 525.
[38] Vitells O. and Gross E., *Astropart. Phys.*, **35** (2011) 230.
[39] Junk T., *Nucl. Instrum. Meth. Phys. Res. A*, **434** (1999) 435.
[40] Read A. L., *J. Phys. G*, **28** (2002) 2693.